Digital holographic microscopy: a novel tool to study the morphology, physiology and ecology of diatoms

EVA-MARIA ZETSCHE[1*‡], AHMED EL MALLAHI[2] & FILIP J. R. MEYSMAN[3, 1]

[1]Analytical, Environmental & Geo-Chemistry, Vrije Universiteit Brussel, Brussels, Belgium

[2]Microgravity Research Centre, Université Libre de Bruxelles, Brussels, Belgium

[3]Department of Ecosystem Studies, Royal Netherlands Institute for Sea Research (NIOZ), Yerseke, The Netherlands

[‡]Present address: Department of Ecosystem Studies, Royal Netherlands Institute for Sea Research (NIOZ-Yerseke), Yerseke, The Netherlands

*Corresponding author. Email: eva-maria.zetsche@nioz.nl

Abstract

Recent advances in optical components, computational hardware and image analysis algorithms have led to the development of a powerful new imaging tool: digital holographic microscopy (DHM). So far, DHM has been predominantly applied in the life science and medical research, and here, we evaluate the potential of DHM within a marine context, i.e., for studying the morphology, physiology and ecology of diatoms. Like classical light microscopy, DHM captures light intensity information from objects, but in addition, it also records the so-called phase information. Because this phase information is recorded in a fully quantitative way, it gives access to a whole new type of image properties, which suitably extends the range of microscopy applications in diatom research. Here, we demonstrate the ability of DHM to provide structural details on internal cell organelles as well as silica frustules of diatoms. By combining the light intensity and phase information, one also obtains the optical 'fingerprint' of a cell, which can be used to discriminate between cells of separate diatom species or to differentiate between living and dead cells (as demonstrated here for two diatom species *Navicula* sp. and *Nitzschia* cf. *pellucida)*. Finally, we use chains of *Melosira* sp. to demonstrate the capacity of DHM to refocus post-acquisition, and combine holograms with fluorescent images, and the ability of DHM to image transparent substances, such as extracellular polymeric substances. Overall, DHM is a promising versatile microscopic technique, allowing diatoms to be investigated in vivo, over time, without the need for staining and quantitatively in terms of their phase information. This way, DHM can provide new insights to the structural details as well as physiology and ecology of diatoms.

Keywords: *diatoms, microscopy, digital holography, quantitative phase imaging, classification, viability*

Introduction

Diatoms are the most ubiquitous group of planktonic organisms and play a major role in the global carbon and silicon cycles (Friedrichs 2013; Lopez et al. 2005). As a major component of the world's phytoplankton communities, they form the basis of marine food webs and contribute at least 20% to the global annual primary productivity (Field et al. 1998). In research on diatom ecology and physiology, microscopy continues to play a crucial role, as it remains the principal tool for the visualization, identification and characterisation of diatom cells. One technique in microscopy is holographic microscopy (HM), which was first described by Gabor in 1948, and soon recognized as a complementary technique to traditional light microscopy (LM), providing valuable additional information and having specific advantages. Foremost, an important known limitation of classical LM is its shallow depth of focus (e.g. only part of a larger organism can be kept in focus; motile cells quickly migrate out of focus). Because a hologram is able to record the optical information in a three dimensional space without loss of resolution, HM enables a far greater depth of focus (typically ten- to a hundred-fold times greater than LM), thus enabling much larger sample volumes to be inspected in one recording (Zetsche et al. 2014). A second important advantage is that objects captured in a hologram can be brought back into focus in a numerical way after the hologram has been recorded (i.e. post-acquisition), a process that is also known as hologram reconstruction (Dubois et al. 2006a; Kemper et al. 2013). Knox (1966) was one of the first to demonstrate this technique, and this application actually occurred within a marine biological context. Different living marine planktonic organisms were imaged at distances

of up to 33 mm from the hologram's original focus plane, and visualized via hologram reconstruction.

In the early decades of holography, plankton studies were one of the important pioneering applications of the HM technique, and diatoms were frequently part of the plankton samples that were studied. Beers et al. (1970) used holograms as a way to image and store permanent records of microplankton samples. Similarly, Almeida et al. (1971) presented holography as a complementary tool to LM for the study of microscopic planktonic organisms such as diatoms. Finally, Cairns et al. (1977; 1982) demonstrated that reconstructed holograms can be used as optical spatial filters in the identification and classification of diatoms. However, at the time, the imaging of individual diatom cells was a laborious procedure requiring specific filters for individual species. As a consequence, HM approaches proved more time-consuming than initially anticipated, and the HM technique was not further pursued for rapid diatom identification.

Since then, work on diatoms (and other plankton species in general) with HM has been very limited. Over the last decade however, there have been major developments in optical components and digital processing capabilities, such as increases in the recording speed and resolution of optical cameras, and the drastic increase in the processing capacities of computers. These advances have also impacted holography and have led to the recent development of digital holographic microscopy (DHM). A new generation of DHM instruments are now available, which enable entirely new applications (e.g. Kemper et al. 2013); they have been successful in various disciplines within the bio-medical and life sciences, including dynamic cell biology, cancer research as well as drugs and toxicity testing (Alm et al. 2011; Kemper et al. 2013; Merola et al. 2013). Clearly, these new DHM technologies also show promising applications in the marine sciences (Katz and Sheng 2010), but applications have been limited. In the few DHM

studies that have imaged diatoms, these diatoms were solely employed as a "test organism" to verify the performance of optical systems (Guehrs et al. 2010; Heine et al. 2011) with no specific interest in gaining information on the diatoms themselves. One exception was the work by Di Caprio et al. (2012), in which the photonics of diatom frustules was investigated with digital holography, thereby looking at how the frustule's pores and valve affected the light distribution within the cell.

One feature that has particularly attracted attention in the biomedical field is the ability of DHM to obtain quantitative phase information (Alm et al. 2013; Kemper et al. 2013; Zetsche et al. 2014). Light is a wave that has both an amplitude and a phase: while LM only records the light intensity (or amplitude), DHM captures both these components. The phase information has been shown to reflect changes in important physiological and biophysical cell parameters (for example, in neuronal cell bodies (Pavillon et al. 2010)), and as a result, the quantitative recording of phase information is seen as a valuable and promising research tool in the life sciences (Alm et al. 2011; Kemper and Schnekenburger 2011). Yet, similar work in the aquatic sciences has not been performed. Recently, we investigated the potential of DHM for the classification of nanoplanktonic organisms and achieved high classification success rates of >90% for nanoplanktonic organisms (Zetsche et al. 2014). The three nanoplanktonic organisms involved in this study, were indiscriminate to the naked eye and LM, but were successfully differentiated with DHM, showing the potential for DHM in the aquatic sciences.

Here, we investigate whether and how DHM can be used as a tool for studying diatoms. Compared to LM, DHM provides several important advantages to study diatoms, including (1) the measurement of quantitative phase information, (2) the ability to perform hologram reconstruction and refocus objects that are recorded out-of-focus, (3) the ability to observe

organisms in vivo, (4) the ability to visualize transparent substances in a water matrix, and, (5) the ability to make observations over time. We present the results of six experiments using two different DHM instruments to highlight the instruments' potential for studies of diatom morphology, physiology and ecology, and we further detail the advantages of post-acquisition hologram reconstruction.

Materials & Methods

Instrumentation - Digital holography

Two different types of holographic instruments were used in this study: (1) the '*oLine D³HM*' stand-alone DHM instrument (hereafter referred to as D³HM), and (2) the '*QMod*' add-on module for standard microscopes. Both instruments have been developed by Ovizio Imaging Systems NV/SA (Belgium) and are provided with the accompanying '*OsOne*' software. The D³HM is a stand-alone DHM instrument implemented with a red LED light source (630 nm). For this study, the D³HM was equipped with a 40x magnification (Leica HCX PL FLUOTAR L 40x/0.60 CORR), although other dry lenses of different magnifications (maximum 40x) can be implemented. The QMod is an add-on holographic module, which is fitted onto a standard upright microscope via a C-mount connection (i.e., same connection as when fitting a digital camera to the microscope). In this study, the QMod was used with a Zeiss Axioplan epifluorescent microscope with a range of dry (objectives 10x, 20x, 40x, 63x) as well as 100x oil lenses and a Nikon Labophot-2 with a 40x magnification. Both holographic instruments were interfaced with the accompanying '*OsOne*' software, which allows the recording of both still images and videos. In 'live' mode the hologram is seen on the computer monitor, and once captured, each hologram is computationally processed. This then provides three computationally

derived images in addition to the original hologram: the light intensity image, the phase image and a false-coloured 3D rendition of the phase (Fig. 1).

Both the D^{3}HM and QMod instruments are based on the principle of differential DHM, whereby an off-axis self-interference approach similar to Fu et al. (2010) provides the holographic information. The principle of DHM with an off-axis holographic approach is discussed in detail in Zetsche et al. (2014), and so here, we only provide a concise summary. A hologram (Fig. 1A) is an interference image that records the information when a light beam is passing through an object (such as a diatom as illustrated in Fig. 1). After the light has passed the object, it can be modified in two principal ways. Firstly, a photon can be absorbed or scattered by the object, thus generating differences in light intensity between various parts of the object (this pattern is what is also recorded in classical LM). Secondly, as the refractive index changes between the object and the surrounding medium, this generates differences in the so-called phase of the transmitted light. This phase information is also recorded by DHM and reveals differences in the optical path length (OPL) across an object, which essentially comprises a measure of how photons are slowed down in a differential way in various parts of the object. Both the intensity information and the phase information are embedded in the original hologram (Fig. 1A). The basic task of the hologram processing software is to extract these two types of information from the recorded hologram, thus providing the intensity image (Fig. 1B) and the phase image (Fig. 1C). Each change in grey level in the phase image represents a nanometric change in the OPL. Because the human eye cannot detect such minute differences in grey level contrast, phase images are typically not presented in their original grey level configuration but are represented in false-coloured 3D renditions (Fig. 1D). This way, small differences in OPL can be visualized, and this then allows to discriminate different cell structures in terms of their OPL.

The OsOne software is used (1) to manage and steer the hologram capture process, and (2) to extract the intensity and phase images from the original hologram, but (3) it additionally includes a range of tools and features to analyse and archive these resulting images (e.g. cell counting, confluence analysis, etc.). Images can also be exported and further analysed with external image analysis software such as MATLAB® or Fiji (Schindelin et al. 2012).

Experiment 1: Post-acquisition refocusing capability

Frequently, organisms such as diatoms are investigated under microscopes on a glass slide. However, these diatom cells, and even more so, chains of cells or filaments, typically do not settle on these microscope slides in one single focus plane. The problem of a limited depth of focus is a known restriction of classical LM. Only cells that are located within a very specific narrow focus plane (typically ~1 µm for a 40x objective) will be captured sharply by the (digital) camera. Applications, such as the automated detection and classification of planktonic cells, however, require sharp images of cells (El Mallahi et al. 2013) . This is because so-called 'features', i.e., parameters extracted from cell images such as cell perimeter and axis length cannot be reliably quantified from out-of-focus images. As noted above, with holography approaches, it is possible to bring out-of-focus cells into focus post-acquisition by computational means using algorithms based on the Kirchhoff–Fresnel propagation equations (Dubois et al. 1999; Yamaguchi and Zhang 1997). This refocusing ability increases the depth of focus considerably.

Here, we used a 40x objective, which provided a depth of focus of ~20 µm (hence 20x times larger than LM) to investigate the refocusing capabilities of the D^3HM instrument. To this end, chains of the diatom *Melosira* sp. (CCY0407) obtained from the Culture Collection Yerseke

(CCY, NIOZ-Yerseke, The Netherlands, http://www.ccy.nioz.nl) were grown on MDV medium at 14°C on a 16:8 light:dark cycle. *Melosira* cells suspended in their medium were then mounted on standard microscope glass slides and protected with cover slips before being viewed with the D^3HM.

Experiment 2: Diatom morphology

Diatom species have very different morphologies and structural features. In this experiment, we examined the imaging capabilities of both the D^3HM and QMod instruments, and particularly, the measurement of quantitative phase information for the visualization of the morphology and internal structure of diatoms i.e. the cell's optical 'landscape'. Both live diatoms as well as cleaned frustules (often used in technological applications) were examined. Live cultures of three diatom species were obtained from the Culture Collection Yerseke: *Melosira* sp. (CCY0407), *Navicula* sp. (CCY0311) and *Phaeodactylum tricornutum* (CCY 0033), which were all grown on MDV medium at 14°C on a 16:8 light:dark cycle. Samples of acid-cleaned diatom frustules of *Pinnularia* sp. were provided by Erik van Eynde (University of Antwerp, Belgium). Frustules of cleaned *Pinnularia borealis* were obtained from Pieter Vanormelingen (University of Gent, Belgium) by harvesting a culture in late-exponential or early-stationary phase and oxidizing the organic material using 37% nitric acid (addition of about half of the harvested volume of cell suspension). The oxidized material was repeatedly washed with distilled water before being mounted in Naphrax (PhycoTech, St. Joseph, USA).

Experiment 3: Physiological status of diatom cells

Within the multi-cellular chains of *Melosira* sp., individual cells frequently contain a varying number of chloroplasts and other cytoplasmic organelles, and so cells show a varying level of internal 'packing' (Bedoshvili et al. 2009; Biggs and Kilroy 2000). Often, some cells within the chain also appear empty and potentially inactive. Thus one can observe a range of cells of different physiological status (live, active, inactive or dead) within a chain. In addition, *Melosira* chains also frequently show so-called mucus pads, which bind the cells together (Horner 2002). Given that DHM provides quantitative phase information, we measured various profiles of the OPL with the D^3HM instrument across these different types of cells to demonstrate how the level of 'packing' as well as the biomaterial type (i.e. cellular material versus mucus pads) can be reflected in phase information differences.

Experiment 4: Combining DHM and epifluorescence

The chain-forming diatom *Melosira* sp. (CCY0408) was further imaged with the QMod mounted on a standard epifluorescent microscope, a Nikon Labophot-2 with a 40x magnification. The QMod is able to capture holograms but also fluorescence images. Chlorophyll *a* fluorescence, in simplified terms measures the photosynthetic capacity of a diatom and is determined in the red spectrum of visible light (peaking at 676 nm); subsequently, a fluorescence filter with excitation at 450-490 nm and emission at ≥520 nm was used. Each image of fluorescence was merged with the processed images of the hologram captured for the same field of view.

Experiment 5: Cell viability assessment

Changes in packing, chlorophyll content or other cellular organelles within a cell may be even more pronounced between live and dead cells. The combined light intensity and phase information provides a 'holographic fingerprint' of the cell, which is defined as the total set of features that can be extracted from the light intensity and phase images. To examine whether this holographic fingerprint can aid in the discrimination between live and dead cells, we performed an experiment with two different diatom species. *Nitzschia cf. pellucida* (DCG 0303), was grown on a f/2 medium at 14°C on a 16:8 light:dark cycle and *Navicula* sp. (CCY0311) was grown on MDV medium and with the same light and temperature settings. To obtain holograms of both live and dead cells, samples of both diatoms were mounted on standard microscope glass slides and protected with cover slips. Approximately 240 cells of *N. pellucida* and 70 cells of *Navicula* were imaged in their healthy state (i.e. 'live') with the QMod in their optimal focus plane. Subsamples from each of the two cultures were then transferred to Eppendorf tubes and heat killed by immersion in a water bath at 50°C for 15 min. The same numbers of images was then captured with the QMod setup for each species, and are hereafter referred to as 'dead' cells. Using the OsOne software, the corresponding intensity and phase images for each individual diatom cell were derived from the recorded holograms and subsequently used for classification analyses.

The cell classification procedure was similar as in Zetsche et al. (2014). Each of the two species cultures was analysed separately. The intensity and phase images were analysed with MATLAB® to first identify an individual cell in an image, which was then isolated and segmented (to remove the background data). In a previous study with nanoplanktonic organisms, phase image features in the holographic fingerprint were shown to be far more discriminative than the light intensity features for the differentiation of species (El Mallahi et al. 2013; Zetsche et al. 2014) and that a combination of 18 morphological and textural features led to the best

classification rates. The same 18 different features were also measured here for each cell as described in Zetsche et al. (2014), including 6 morphological features (area, major axis, minor axis, perimeter, equivalent circular diameter and eccentricity) from the light intensity images and a set of 6 textural features (average grey level, average contrast, smoothness, skewness, uniformity and entropy) each from both light intensity and phase images. The values for each of the 18 features were then used in a supervised classification procedure using support vector machines to be able to test how well live cells could be differentiated from dead cells using these features. Details on this procedure are given in Zetsche et al. (2014). The supervised classification procedure allows us to categorize the cells as being either live or dead, and a classification score of 100% would imply that all cells have been correctly classified.

In addition, differences for each feature between live and dead cells were statistically analysed using the statistical analysis routines incorporated into SigmaPlot 13.0 (Systat Software Inc., USA) while using a level of significance of $p<0.05$. Since assumptions of normality and/or homogeneity of variance failed on most of the dataset, non-parametric Mann Whitney tests were used.

Experiment 6: Biofilm formation

DHM has the ability to image transparent substances (Kemper et al. 2013; Zetsche et al., under review) and to observe processes over time. Diatoms are known to excrete extracellular polymeric substances (EPS) and can form dynamic biofilms in which they are constantly migrating (Aumeier and Menzel 2012; Hoagland et al. 1993). To examine these processes, we used a diatom culture of *Nitzschia capitellata*, which was obtained from the Culture Collection NIOZ-Texel (The Netherlands) and kept in culture in 50 mL plastic bottles (TPP, Switzerland)

with f/2 media, under a 16:8 light:dark cycle at 20ºC with lysate. Over time the diatoms developed a biofilm on the culture bottle's bottom surface encompassing the cells. Cells and the surrounding biofilm were loosened by shaking and a subsample pipetted onto a glass slide and imaged with the D^3HM. Diatom motility and behaviour within this piece of biofilm was followed for several minutes and recorded as images.

Results

Experiment 1: Post-acquisition refocusing capability

Melosira sp. is a chain-forming diatom species, and when visualized under a microscope, cells commonly do not line up in one single focus plane. DHM allows us to image the whole chain in one hologram, and subsequently, via hologram reconstruction, it becomes possible to image the individual cells of the chain in their optimal focus plane. Fig. 2 illustrates this capability of refocusing post-acquisition: the focus plane of the cell marked with the white arrow in Fig. 2A is at the correct focus plane, i.e., it was in focus when capturing the hologram. However, the cells to the left and right remain out-of-focus. By offsetting the focus plane in the Z-direction (this was done post-acquisition using the OsOne software), we obtained the optimal refocusing plane for different cells (Fig. 2C–D). This refocusing procedure was repeated here for each of the different focus planes in which the cells of the chain are present, and is exemplified for a depth of -10 and -15 µm from the original focusing plane. Algorithms have recently been developed that automate this refocusing procedure (El Mallahi and Dubois 2011; Kemper et al. 2013).

Experiment 2: Diatom morphology

The optical path length (OPL) of an object is principally determined by two factors: the material type as well as the height of an object. To compute the physical height (h) of the object from the OPL, one needs information on the refractive index (n) of the material. For a uniform material, the height can be determined as: $h = OPL/\Delta n$, where Δn is the difference of refractive index between the medium and the sample. In general, however, a diatom cell will not have a uniform refractive index in a given cross-section, as the refractive index of the cytoplasm, the cell membrane lipids and the silica test will be different. Accordingly, one cannot translate OPL data acquired by DHM into "real-world" information about the height of cells without specific assumptions about the refractive index. Still, the variation in the OPL across a given cell provides valuable information on the structural organization within the cell.

Digital holography allows the construction of an accurate 3D rendition of the OPL of a diatom cell, which enables the visualization of the structural organization of diatoms in terms of cellular components, shapes and features (Fig. 3). This applies to both, living diatom cells (Fig. 3A–C) as well as the silica structure of acid-cleaned diatom frustules (Fig. 3D–F). Given that phase information obtained with DHM is quantitative, it becomes possible to quantify differences in the OPL "landscape" between various species, but also to quantify differences in OPL between the internal structures within a single cell. Lipid bodies are clearly observed in the cell of *Phaeodactylum tricornutum* (Fig. 3C), a species that is being intensely researched for its ability to produce these lipid bodies given its importance for algal biofuel production. The OPL across the lipid bodies is ~0.6 µm compared to across its other visible internal cell organelles (most likely chloroplasts, ~0.35 µm). In Fig. 3A we also see differences in OPL for *Melosira* sp. cells compared to mucus pads that are connecting different cells within the stain (further discussed in Experiment 3 below).

The quantitative phase information represented in the 3D renditions can also be used in a comparative way. For example, the mean OPL measured for *Navicula* cells (Fig. 3B) is approximately 0.19 µm (range between 0.10 and 0.30 µm; calculated from transects drawn along the longest axis of each of the three cells in Fig. 3B). In comparison, *P. tricornutum* cells have a higher mean OPL of 0.38 µm, ranging between 0.35 and 0.45 µm, whilst *N. pellucida* cells have an even higher mean OPL of around 0.44 µm. Such simple measurements of the maximum OPL across a length profile show how quantitative information can be extracted from phase images. In a similar fashion, other cell characteristics and features can be extracted and used for cell analysis (see Experiment 5).

Cleaned diatom frustules are used in various technological applications, and for this, it is important to characterize the morphology of these frustules. Figure 3D–F shows how DHM can be used to this purpose. Both acid-cleaned diatom frustules of *Pinnularia borealis* (Fig. 3D) and *Pinnularia* sp. (Fig. 3E) reveal details of the diatoms' silica skeleton after successful cleaning procedures. A sample of the same *Pinnularia* sp. in Fig. 3F has been cleaned and dried with an alternative procedure (using H_2O_2), and showed incomplete removal of the cell's organic material.

Experiment 3: Physiological state of cells

As mentioned before, cells of *Melosira* sp. within a chain frequently differ in terms of their chlorophyll 'packing volume', and are also often connected by mucus pads. Since the phase information collected with the DHM instruments is quantitative we can compare the OPL of the mucus pads between the cells. We observed that these values are within a narrow range for different chains of *Melosira* cells that were analysed. Transect measurements across mucus pads

showed that the OPL ranged between 0.3 and 0.35 µm (Fig. 4). This contrasts with OPL transect measurements across chloroplasts inside cells. The maximum OPL observed for a profile across a cell ranged between 0.7 and 0.8 µm for fully packed cells, but was much smaller (maximum OPL ~0.2 µm) for partially 'packed' cells. The OPL profile for partially packed cells also reflects the inhomogeneity of chloroplasts across the cell (Fig. 4).

Experiment 4: Combining DHM and epifluorescence

The QMod was mounted on a standard epifluorescent microscope, allowing us to combine DHM measurements with fluorescence microscopy (Fig. 5). Chlorophyll *a* was detected and imaged with the QMod as fluorescence images which were merged with the processed images of the hologram taken of the same field of view. Applying this technique to chains of the diatom *Melosira* sp., we produced overlay images of the DHM phase and intensity images with the *Melosira* autofluoresence (Fig. 5). This way, we could combine the detection of active fluorescence with visual information on the internal cell structures, as derived from the intensity images, but more so, from the phase images obtained from the QMod (Fig. 5). We observed clear differences in the packing of chloroplasts within cells along the chain. Some of the cells were not autofluorescent, most likely being in a state of decline (Fig. 5E-F). Cells 1-4, as indicated in Fig. 5E, showed shrunken chloroplasts, which were not fully functional anymore, and thus lost their autofluorescence. Weak autofluorescence was still seen in cell 1, less in cell 2 and none in cell 3 and 4, which clearly had few chloroplasts left. Interstitial mucus pads were also observed in the chain, which did not fluoresce, and can thus be clearly distinguished from the cells, particularly in using the information from the phase image (Fig. 5C).

Experiment 5: Viability determination

Distinct differences in the phase image were observed between live cells and cells from the same culture that were heat-killed (Fig. 6), suggesting that the phase information can be useful in quantitatively assessing the viability of diatoms. The OPL landscape of a cell was clearly affected by heat-killing. As seen in Fig. 6C and F, by drawing an OPL profile across the longest axis of the cells, live cells consistently had one distinct trough in the middle of the cells between the chloroplasts. For heat-killed cells, OPL varied across the cell's landscape with no consistent patterns and was low over extensive areas (Fig. 6C,F).

Statistical analysis additionally confirmed that heat-killing alters the holographic fingerprint, i.e., the set of 18 morphological and textural features that are extracted from the light and phase intensity images. However, this was mainly due to an impact on textural features, as morphological features extracted from the light intensity image did not differ consistently between live and dead cells for either of the two diatom species investigated. Large differences in the morphological parameters between live and dead cells are not expected for diatoms, as the frustule will remain the same - dead or alive. Two of the six morphological features were not significantly different (Fig. 7A) between live and dead *N. pellucida* cells, whilst five of the six features were not significantly different between live and dead *Navicula* cells. The cell perimeter was the only feature that changed significantly for both *N. pellucida* and *Navicula* cells ($p<0.01$). Most likely the cell perimeter increased in both species as lysing cells had lost their internal structural organization due to the heat-killing treatment. In contrast, all textural features calculated on both light intensity and phase images differed significantly, as shown for *N. pellucida* in Fig. 7 (results for *Navicula* are similar and not shown).

Supervised classifications were run for each species and for different types and combinations of features: using (a) morphological features only, (b) textural features from the light intensity images only, (c) textural features from the phase images only, (d) all textural features (both light intensity and phase), and (e) a combination of all 18 features (both morphological as well as textural). When only the morphological features were used, the classification of cells led to low overall classification success rates of 69.5% and 68% for *N. pellucida* and *Navicula* cells, respectively (Table 1). These overall rates are averages of the results from the live and dead cell classification, but live cells tended to be classified better than dead cells at all times. Cell shapes of live cells were always well defined, whereas degradation processes led to random discontinuities within the dead cells irrespective of the segmentation process (i.e., more variation within a cell's contour). Textural features proved more powerful for differentiating live from dead cells, while the textural features obtained from the phase images gave a slightly better result than classification based on textural features from the intensity images. However, it was the combination of textural features from both light intensity and phase images that gave the best classification rates – 96% and 95% for *N. pellucida* and *Navicula* cells, respectively. When all 18 features of the holographic fingerprint were included, the classification success again decreased to 80.5% and 85% for *N. pellucida* and *Navicula* cells, respectively (Table 1).

Experiment 6: Biofilm formation

Biofilms formed by *Nitzschia capitellata* were mounted on a glass slide, and the movement of the diatoms through this biofilm could be tracked (Fig.8B–C). Within this biofilm, the accretion of extracellular polymeric substances in the trails of the moving diatoms were most

clearly visible in the false-colour phase images, which illustrates the ability of DHM to visualize transparent mucoid substances in a water phase (Fig. 8E–F). Strong differences in the OPL of the diatom trails were observed. Values were taken from the four transect profiles depicted in Fig. 8C; the diatom trails had very small OPLs of 0.003 and 0.02 µm, compared to the OPLs of the moving *N. capitellata* cells themselves, measured at 0.34 and 0.42 µm.

Discussion

Microscopy remains a principal tool for the visualization, identification and characterisation of diatom cells. Our results show that DHM is a versatile microscopic technique, which is complementary to traditional light microscopy due to its additional quantitative recording of the phase information. As shown here, DHM enables new ways of visualizing the internal structural details and excretions of diatoms, and thus its application can provide new insights into the physiology and ecology of diatoms.

Structural aspects of diatoms imaged with DHM

Diatom studies (and plankton studies in general) try to capture the unique and fine detailed structures of diatoms, but are hampered by the transparency and lack of colouration of cells (Höbel and Sterrenburg 2011; Piper 2011). Apart from the chloroplasts, diatom cells are for the large part transparent, and since transparent substances or objects – by definition – do not absorb light in appreciable quantities when suspended in a seawater solution, these entities are hard to discriminate and detect by microscopy techniques that only rely on intensity information. The refractive index of cell organelles or excreted polymeric substances often differs only slightly to that of the surrounding medium, making it difficult to obtain images of good contrast.

Piper (2011) suggested that interference-based contrast microscopy reveals the shape and structure of cells more clearly, as it improves the plasticity and contour sharpness. DHM is such an interference-based approach, and as our results show, DHM enables to more clearly define the structural organization of diatoms in terms of cellular components, shapes and features (Fig. 3).

DHM overcomes some of the restrictions of LM by recording both the amplitude as well as the phase information (Di Caprio et al. 2012; Hobson and Watson 2002), and allowing the phase information of an object to be quantified (Dubois et al. 2006b). As a result, DHM can detect subtle changes in the OPL within a single cell, or variations in OPL between different cells. We recorded differences in mean OPL between various diatom species in the order of only several tens of nanometers (Fig. 3), or of several hundreds of nanometers between cells within a single chain of *Melosira* sp. due to differences in the number of chloroplasts present (Fig. 4). The internal cell structure is clearly distinguished in the images obtained with both the D^3HM and the QMod (Figs 3–4). As noted above, the OPL depends on the difference in refractive index (Δn) between the medium and the sample. Hence, embedding the same sample in a different medium will change the OPL, as the refractive index of the medium changes (e.g. a change in embedding of the sample from water to oil). However, within the same medium, OPL differences are fully comparable, and moreover, this OPL information should not be instrument dependent (hence the OPL data can be compared to quantitative phase contrast microscopes and other digital holographic microscopes).

A typical diatom cell is composed of protoplasm containing its internal organelles (e.g. chloroplasts, nucleus, lipid bodies), which is surrounded by an inorganic cell wall or 'frustule'. Diatom frustules are intricate, self-assembled porous silica cell walls with very specific 3D morphologies. In recent years, interest in the diatom's silica structure has grown for applications

in nanotechnologies and materials science (Friedrichs 2013; Lopez et al. 2005). The size and symmetry of diatoms as well as their lightweight structural constructions has inspired engineers and materials scientists in a diverse range of applications, ranging from micro-electromechanical systems, nanoclasps and functional microdevices to nanostructured composite ceramic materials (Hamm 2005; Lopez et al. 2005; Tiffany et al. 2010). Cleaned diatom frustules, such as those examined here (Fig. 3D-F), are modified and used as biosilica-titania photocatalysts in air purification applications, after impregnation of the frustules with varying amounts of titanium dioxide (Van Eynde et al. 2013). Clean intact frustules are a requirement for these types of applications and DHM can help in the rapid identification of how well remaining organic cellular material is removed or cells are destroyed with different known cleaning protocols (data not shown). The diatom frustules shown in Fig. 3E and F have been processed with two different cleaning methods (HNO_3 versus H_2O_2), and the remaining frustules show a different OPL landscape, suggesting a less efficient removal of organic cell wall material in the H_2O_2 treatment, and hence cleaner frustules in the HNO_3 treatment. The availability of quantitative OPL landscape data provided by DHM opens the possibility to quantitatively compare the efficiency of these treatments. This way, further studies could help in advancing new applications for diatom frustules within a technological context using DHM technology.

DHM visualizes EPS and mucoid substances

The capability of DHM to visualize transparent cells and transparent polymeric substances has already been demonstrated in medical and life science research (Alm et al. 2011; Kemper et al. 2013). In this context, one of the main advantages of DHM is that it does not require the use of stains for imaging transparent substances. Kemper et al. (2013), for example,

demonstrate how glycerol is injected into a phosphate-buffered saline, and subsequently, fluid movement and mixing is observed with much greater contrast when using DHM compared to the white light microscopy. DHM does not require cells or substances of interest to be fixed or dried, does not need to be operated under vacuum and provides non-contact imaging. More recently, Zetsche et al. (under review) demonstrated the use of DHM for observing mucus production by the cold-water coral *Lophelia pertusa*. Coral mucus predominantly consists of polysaccharides and proteins, similar to extracellular polymeric substances (EPS) and other mucoid substances typically extruded by diatoms. Here, we successfully imaged the transparent mucus pads of *Melosira* sp. and were able to compare their OPL to those of the actual diatom cells (Fig. 4). Furthermore, we presented images of a biofilm and the movement of diatom cells therein (Fig. 8). EPS may be released by diatoms for a variety of reasons, including the adhesion and movement of the cells (Higgins et al. 2003; Poulsen et al. 1999), the creation of localised microenvironments and cell signalling as well as pathogen-host interactions (Bhaskar and Bhosle 2005; Bhinu 2006; Underwood 2010). Since the late 1990's, biofilm formation and associated EPS production has been studied predominantly using fluorescent stains in combination with epifluorescence microscopy and confocal laser scanning microscopy (CLSM) (Strathmann et al. 2002). Despite these being non-destructive methods and allowing structures and organisms to remain intact, once stained, samples are fixed and cannot be observed across longer periods of time. Using the quantitative phase information generated by our DHM instruments we were able to visualize the optical height of diatom trails as they were formed by the moving cells within a biofilm (Fig. 8). Overall, DHM allows to observe transparent substances such as EPS over time in a non-invasive manner, and thus could improve our understanding of processes such as biofilm formation.

The diatom species *Navicula, Nitzschia* and *Melosira* that were imaged in this study have all been classed as marine fouling diatoms, i.e., species that incur important economic costs by adhesion and biofilm formation onto ship hulls and engineering structures deployed in the marine environment (Holland et al. 2004; Molino and Wetherbee 2008). Gaining a better understanding of these diatoms, their adhesion capabilities and biofilm formation processes is critical in many aspects and a major driver of applied plankton research. Heine et al. (2011) already demonstrated the ability of a different holographic approach (digital in-line X-ray holography) to image the cells of a similar diatom, *Navicula perminuta,* a common biofouling diatom prevalent on contemporary foul release coatings (Holland et al. 2004). This holographic imaging provided access to chemical and structural information of the diatom to better understand its surface adhesion and adhesive production (Heine et al. 2011). Future studies using digital holographic techniques may involve the study of EPS and mucus release mechanisms over time, and may focus on EPS production and biofilm formation in less constricted settings than a microscope slide.

Advantages of DHM

DHM is advantageous for various cell studies because cells can be observed alive, over time and without the need for staining allowing dynamic movements to be detected (Alm et al. 2011; Kemper et al. 2013; Kemper and Schnekenburger 2011). In addition, the use of a LED light source in the D^3HM instead of a laser also reduces possible photo-toxic effects often associated with long exposures to laser light sources (Dobrucki et al. 2007). The D^3HM also does not require samples to be mounted on slides, but can also be utilized for the observation of cells over time *in vivo* in petri dishes, well plates, flow cells, and similar containers (Barbau et al.

2014; Dubois et al. 2006b). Subsequently, dynamic processes may be studied in detail such as cell growth and division, biofilm formation as well as cell and species interactions.

A key advantage of DHM systems is the ability to process the same single hologram many times over. This allows the user to find the best focus plane for each individual cell via hologram reconstruction, so that all targeted cells are brought into focus (Fig. 2). This post-acquisition refocusing is a major advantage of DHM compared to other microscopy techniques, as it ensures that cell features can be reliably and accurately extracted, which for example, greatly improves the identification and classification (Alm et al. 2011; El Mallahi et al. 2013; Zetsche et al. 2014).

In this study, we have used both a stand-alone DHM instrument (D^3HM) as well as an add-on module for standard microscopes (QMod). The resolution of the details that is achieved with each system ultimately depends on the optical system i.e. using the same kind of objective (NA) gives a similar system resolution. The stand-alone DHM version is more versatile in the type of samples that can be imaged. In addition to normal glass microscope slides, the D^3HM can hold and image experiments using petri dishes, well plates, culturing containers and flow-through cells. The ability to add a DHM module onto an existing fluorescence microscope has other advantages.

Through the QMod add-on module, DHM was here combined with standard fluorescence microscopy. Fluorescence was used for highlighting a certain part of the cell, i.e. the autofluorescence of chloroplasts, which provided insight into chloroplast packing and photosynthetic activity in chain-forming diatoms (Fig. 5). Healthy and dividing chloroplasts show autofluorescence, but decaying cells lose it very quickly (within minutes) (Dijkman and Kromkamp 2006). Shrunken chloroplasts may not be fully functional anymore or lose their weak

autofluorescence quickly by quenching, thus likely causing the weakened autofluorescence in cells 1-4.

Fluorescence microscopy could be further combined with DHM in other ways to better understand the physiological processes occurring in a cell. Shimizu et al. (2001), for example, introduced a fluorescent marker compound into diatom cells to visualize the ongoing silica deposition. Similarly, other markers such as BODIPY are used to confirm the presence of lipid bodies in algal cells, including diatom species (Govender et al. 2012; Prakasam and Elumalai 2011). The study of lipid body formation in algae is an important aspect in the race for efficient algal biofuel production (Scott et al. 2010). Lipid bodies are clearly defined in the phase image (Fig. 3C), and the lipid content then can be further verified with the appropriate fluorescent markers and filters.

Stain-free viability determination

Typical procedures for the determination of cell viability currently rely on staining with various fluorescent markers (Veldhuis et al. 2001). Here, we have illustrated a DHM-based procedure for discrimination between live and dead cells that does not need staining, a technique that is already known and used in the life sciences (Alm et al. 2013; Kemmler et al. 2007; Kemper et al. 2006). A combination of extracted features from the intensity images and phase images provided a high classification success rate (> 95%) for live and dead cells. Distinct differences in the phase image were critical to successfully assess the viability of a cell, clearly showing that the modification of the internal cell structures upon lysis is suitably reflected in the phase image textural features of the cells. Future experiments using algal cell mixtures as well as unsupervised classification routines will further substantiate this capability of the DHM for live-

dead discrimination of plankton, as well as species identification and classification. Certain species of diatoms are frequently used for monitoring purposes to assess the water quality of rivers and lakes as well as coastal areas (Antón-Garrido et al. 2013; Kelly et al. 2009; Sabater et al. 2007), and so, DHM may facilitate the live-dead differentiation of cells and thus improve these monitoring capabilities.

Conclusion

We have presented two instruments based on DHM technology (the 'oLine D^{3}HM' and the 'QMod') that extend the diatom toolbox with new microscopic methods and capabilities. These instruments are both robust microscopic systems that allow the observation of diatoms in a preserved state as well as in vivo. Cells can be observed and imaged when mounted on standard microscopy slides or in larger containers such as multi-well plates and petridishes (data not shown). The versatility of DHM enables observations of both static as well as dynamic processes, and provides us with both intensity-based as well as phase-based data. We demonstrated for the first time that a differentiation between live and dead diatom cells can be made based solely on image analysis procedures without any preceding staining procedures. Furthermore, we observed the trail formation of diatoms as they moved within a biofilm. These example applications affirm the potential of DHM instrumentation to improve our understanding of morphological, ecological as well as physiological aspects of diatoms.

Acknowledgements

We are indebted to Michele Grego (Culture Collection Yerseke, Royal Netherlands Institute for Sea Research) for his algal culturing work, as well as Cátia Carreira and Corina

Brussaard (Royal Netherlands Institute for Sea Research, Texel) for providing a sample of *Nitzschia capitellata*. We also thank Erik van Eynde (University of Antwerp, Belgium) and Pieter Vanormelingen (University of Gent, Belgium) for providing samples of diatom frustules. Finally, we thank Ovizio Imaging Systems for providing general support as well as access to the QMod instrument.

Funding

This work was supported by The Brussels Institute for Research and Innovation (INNOVIRIS) in the framework of the HoloFlow Impulse-Environment Project. F.J.R.M. was further supported by the European Research Council through ERC Grant 306933.

References

ALM K.et al. 2011. Digital holography and cell studies. In: *Holography: Research and Technologies* (Ed. by [ed.]^[eds.]). InTech.

ALM K., Z. EL-SCHICH, M.F. MINIOTIS, A.G. WINGREN, B. JANICKE, and S. OREDSSON 2013. Cells and Holograms – Holograms and digital holographic microscopy as a tool to study the morphology of living cells. In: *Holography - Basic Principles and Contemporary Applications* (Ed. by [ed.]^[eds.]).

ALMEIDA S.P., D.R.D. BALZO, J. CAIRNS, JR., K.L. DICKSON, and G.R. LANZA 1971. Holographic microscopy of diatoms. *Transactions of the Kansas Academy of Science (1903-)* 74: 257-260.

AUMEIER C., and D. MENZEL 2012. Secretion in the diatoms. In: *Secretions and exudates in biological systems* (Ed. by [ed.]^[eds.]), pp. 221-250. Springer.

BEDOSHVILI Y.D., T.P. POPKOVA, and Y.V. LIKHOSHWAY 2009. Chloroplast structure of diatoms of different classes. *Cell Tiss. Biol.* 3: 297-310.

BEERS J.R., C. KNOX, and J.D.H. STRICKLAND 1970. Permanent record of plankton samples using holography. *Limnology and Oceanography* 15: 967-970.

BHASKAR P.V., and N.B. BHOSLE 2005. Microbial extracellular polymeric substances in marine biogeochemical processes. *Current Science* 88: 45-53.

BHINU V. 2006. Insight into biofilm-associated microbial life. *Journal of Molecular Microbiology and Biotechnology* 10: 15-21.

CAIRNS J., K.L. DICKSON, and J. SLOCOMB 1977. The ABC's of diatom identification using laser holography. *Hydrobiologia* 54: 7-16.

CAIRNS J., JR., S.P. ALMEIDA, and H. FUJII 1982. Automated identification of diatoms. *BioScience* 32: 98-102.

DI CAPRIO G.et al. 2012. Shedding light on diatom photonics by means of digital holography. *Journal of Biophotonics* 7: 341-350.

DIJKMAN N.A., and J.C. KROMKAMP 2006. Photosynthetic characteristics of the phytoplankton in the Scheldt estuary: community and single-cell fluorescence measurements. *European Journal of Phycology* 41: 425-434.

DOBRUCKI J.W., D. FERET, and A. NOATYNSKA 2007. Scattering of exciting light by live cells in fluorescence confocal imaging: phototoxic effects and relevance for FRAP studies. *Biophysical Journal* 93: 1778-1786.

DUBOIS F., N. CALLENS, C. YOURASSOWSKY, M. HOYOS, P. KUROWSKI, and O. MONNOM 2006a. Digital holographic microscopy with reduced spatial coherence for three-dimensional particle flow analysis. *Applied Optics* 45: 864-871.

DUBOIS F., L. JOANNES, and J.-C. LEGROS 1999. Improved three-dimensional imaging with a digital holography microscope with a source of partial spatial coherence. *Applied Optics* 38: 7085-7094.

DUBOIS F.et al. 2006b. Digital holographic microscopy for the three-dimensional dynamic analysis of in vitro cancer cell migration. *Journal of Biomedical Optics* 11: 054032-054032-054035.

EL MALLAHI A., and F. DUBOIS 2011. Dependency and precision of the refocusing criterion based on amplitude analysis in digital holographic microscopy. *Optics Express* 19: 6684-6698.

EL MALLAHI A., C. MINETTI, and F. DUBOIS 2013. Automated three-dimensional detection and classification of living organisms using digital holographic microscopy with partial spatial coherent source: application to the monitoring of drinking water resources. *Applied Optics* 52: A68-A80.

FIELD C.B., M.J. BEHRENFELD, J.T. RANDERSON, and P. FALKOWSKI 1998. Primary production of the biosphere: integrating terrestrial and oceanic components. *Science* 281: 237-240.

FRIEDRICHS L. 2013. A simple cleaning and fluorescent staining protocol for recent and fossil diatom frustules. *Diatom Research* 28: 317-327.

FU D.et al. 2010. Quantitative DIC microscopy using an off-axis self-interference approach. *Optics Letters* 35: 2370-2372.

GABOR D. 1948. A new microscopic principle. *Nature* 161: 777-778.

GOVENDER T., L. RAMANNA, I. RAWAT, and F. BUX 2012. BODIPY staining, an alternative to the Nile Red fluorescence method for the evaluation of intracellular lipids in microalgae. *Bioresource Technology* 114: 507-511.

GUEHRS E.et al. 2010. Wavefield back-propagation in high-resolution X-ray holography with a movable field of view. *Optics Express* 18: 18922-18931.

HAMM C.E. 2005. The evolution of advanced mechanical defenses and potential technological applications of diatom shells. *Journal of Nanoscience and Nanotechnology* 5: 108-119.

HEINE R.et al. 2011. Digital in-line X-ray holography with zone plates. *Ultramicroscopy* 111: 1131-1136.

HIGGINS M.J., P. MOLINO, P. MULVANEY, and R. WETHERBEE 2003. The structure and nanomechanical properties of the adhesive mucilage that mediates diatom–substratum adhesion and motility. *Journal of Phycology* 39: 1181-1193.

HOAGLAND K.D., J.R. ROSOWSKI, M.R. GRETZ, and S.C. ROEMER 1993. Diatom extracellular polymeric substances: function, fine structure, chemistry, and physiology. *Journal of Phycology* 29: 537-566.

HÖBEL P., and F.A.S. STERRENBURG 2011. UV photomicrography of diatoms. *Diatom Research* 26: 13-19.

HOBSON P.R., and J. WATSON 2002. The principles and practice of holographic recording of plankton. *Journal of Optics A: Pure and Applied Optics* 4: S34.

HOLLAND R.et al. 2004. Adhesion and motility of fouling diatoms on a silicone elastomer. *Biofouling: The Journal of Bioadhesion and Biofilm Research* 20: 323 - 329.

HORNER R. 2002. *A taxonomic guide to some common marine phytoplankton* Biopress Limited. 195.

KATZ J., and J. SHENG 2010. Applications of holography in fluid mechanics and particle dynamics. *Annual Review of Fluid Mechanics* 42: 531-555.

KELLY M.et al. 2009. Uncertainty in ecological status assessments of lakes and rivers using diatoms. *Hydrobiologia* 633: 5-15.

KEMMLER M., M. FRATZ, D. GIEL, N. SAUM, A. BRANDENBURG, and C. HOFFMANN 2007. Noninvasive time-dependent cytometry monitoring by digital holography. *Journal of Biomedical Optics* 12: 064002-064002-064010.

KEMPER B.et al. 2006. Investigation of living pancreas tumor cells by digital holographic microscopy. *Journal of Biomedical Optics* 11: 034005-034005-034008.

KEMPER B.et al. 2013. Digital holographic microscopy: quantitative phase imaging and applications in live cell analysis. In: *Handbook of Coherent-Domain Optical Methods* (Ed. by [ed.]^[eds.]), pp. 215-257. Springer.

KEMPER B., and J. SCHNEKENBURGER 2011. Digital holographic microscopy for quantitative live cell imaging and cytometry. In: *Advanced Optical Flow Cytometry* (Ed. by [ed.]^[eds.]), pp. 211-237. Wiley-VCH Verlag GmbH & Co. KGaA.

KNOX C. 1966. Holographic microscopy as a technique for recording dynamic microscopic subjects. *Science* 153: 989-990.

LOPEZ P.J., J. DESCLÉS, A.E. ALLEN, and C. BOWLER 2005. Prospects in diatom research. *Current Opinion in Biotechnology* 16: 180-186.

MEROLA F.et al. 2013. Digital holography as a method for 3D imaging and estimating the biovolume of motile cells. *Lab on a Chip* 13: 4512-4516.

MOLINO P.J., and R. WETHERBEE 2008. The biology of biofouling diatoms and their role in the development of microbial slimes. *Biofouling: The Journal of Bioadhesion and Biofilm Research* 24: 365-379.

PAVILLON N.et al. 2010. Cell morphology and intracellular ionic homeostasis explored with a multimodal approach combining epifluorescence and digital holographic microscopy. *Journal of Biophotonics* 3: 432-436.

PIPER J. 2011. A review of high-grade imaging of diatoms and radiolarians in light microscopy optical- and software-based techniques. *Diatom Research* 26: 57-72.

POULSEN N.C., I. SPECTOR, T.P. SPURCK, T.F. SCHULTZ, and R. WETHERBEE 1999. Diatom gliding is the result of an actin-myosin motility system. *Cell Motility and the Cytoskeleton* 44: 23-33.

PRAKASAM V., and S. ELUMALAI 2011. Lipid granules staining (Nile Red and Bodipy) of different biofuel producing fresh water microalgae growing under various stress conditions. *Journal of Experimental Sciences* 2.

SABATER S.et al. 2007. Monitoring the effect of chemicals on biological communities. The biofilm as an interface. *Anal Bioanal Chem* 387: 1425-1434.

SCHINDELIN J.et al. 2012. Fiji: an open-source platform for biological-image analysis. *Nature methods* 9: 676-682.

SCOTT S.A.et al. 2010. Biodiesel from algae: challenges and prospects. *Current Opinion in Biotechnology* 21: 277-286.

SHIMIZU K., Y. DEL AMO, M.A. BRZEZINSKI, G.D. STUCKY, and D.E. MORSE 2001. A novel fluorescent silica tracer for biological silicification studies. *Chemistry & Biology* 8: 1051-1060.

STRATHMANN M., J. WINGENDER, and H.-C. FLEMMING 2002. Application of fluorescently labelled lectins for the visualization and biochemical characterization of polysaccharides in biofilms of *Pseudomonas aeruginosa*. *J. Microbiol. Methods* 50: 237-248.

TIFFANY M.A., R. GORDON, and I.C. GEBESHUBER 2010. *Hyalodiscopsis plana*, a sublittoral centric marine diatom, and its potential for nanotechnology as a natural zipper-like nanoclasp. *Polish Botanical Journal* 55: 27-41.

UNDERWOOD G.J.C. 2010. Exopolymers (extracellular polymeric substances) in diatom-dominated marine sediment biofilms. In: *Microbial Mats: Modern and Ancient Microorganisms in Stratified Systems* (Ed. by [ed.]^[eds.]), pp. 289-300. Springer.

VAN EYNDE E., T. TYTGAT, M. SMITS, S.W. VERBRUGGEN, B. HAUCHECORNE, and S. LENAERTS 2013. Biotemplated diatom silica-titania materials for air purification. *Photochemical & Photobiological Sciences* 12: 690-695.

VELDHUIS M.J.W., G.W. KRAAY, and K.R. TIMMERMANS 2001. Cell death in phytoplankton: correlation between changes in membrane permeability, photosynthetic activity, pigmentation and growth. *European Journal of Phycology* 36: 167-177.

YAMAGUCHI I., and T. ZHANG 1997. Phase-shifting digital holography. *Optics Letters* 22: 1268-1270.

ZETSCHE E., T. BAUSSANT, F.J.R. MEYSMAN, and D. VAN OEVELEN Direct visualization of mucus production by the cold-water coral *Lophelia pertusa* with digital holographic microscopy. *PLOS One* (under review).

ZETSCHE E., A. EL MALLAHI, F. DUBOIS, C. YOURASSOWSKY, J. KROMKAMP, and F.J.R. MEYSMAN 2014. Imaging-in-Flow: Digital holographic microscopy as a novel

tool to detect and classify nanoplanktonic organisms. *Limnology and Oceanography: Methods* 12: 757–775.

Table 1. Results of the mean performances of the classification procedure (% ± SD) for the two study organisms and their classification as living or dead. A combination of all textural features led to the most successful classification rate (highlighted in bold).

Organism	Morphological features	Textural features (intensity images)	Textural features (phase images)	**Textural features (intensity+phase)**	All features (textural+morphol.)
Nitzschia cf. pellucida					
Live	95 ± 2	95 ± 1	77 ± 8	**100**	100
Dead	44 ± 6	67 ± 5	86 ± 4	**92 ± 2**	61 ± 5
***Navicula* sp.**					
Live	75 ± 7	89 ± 5	94 ± 3	**100**	92 ± 4
Dead	61 ± 9	58 ± 4	61 ± 7	**90 ± 3**	78 ± 5

Figure captions (as a list)

Fig. 1. (A) Hologram of a cleaned diatom frustule of *Stauroneis* sp. (University of Gent, Belgium) as obtained with a digital holographic microscope (oLine D^3HM). This hologram contains both light intensity information (B) as well as phase information (C) representing the optical path length (OPL) of the object. (D) The OPL of an object is more clearly visualized with false colouring of the phase information.

Fig. 2. Post-acquisition refocusing with the D^3HM of the cells in a *Melosira* sp. chain: (A) A single hologram is recorded of the whole chain of cells with the cell marked by the white arrow in focus. (B) The corresponding intensity image is derived from the hologram in the optimal focus plane for the cell marked by the white arrow. (C) Via hologram reconstruction, the focus plane is shifted by -10 µm to bring a cell to the left into focus (grey arrow). The corresponding intensity image is again derived. (D) A shift by -15 µm from the original focus plane brings the cell marked with the black arrow into focus, and the corresponding intensity image is shown. Note how the original cell (white arrow) gradually loses its focus as the focus plane shifts further away.

Fig. 3. Examples of false-coloured 3D renditions of the quantitative phase information captured with both the D^3HM (A,D–F) and the QMod (B–C) for a number of different diatoms. (A) The chloroplasts of the chain-forming diatom *Melosira* sp. (CCY0407, The Netherlands) often fill the cells to varying degrees, with empty cells being present along the chain. Cells are frequently connected by mucus pads, which are clearly distinguishable in this false-colour image (black arrow). (B) Three *Navicula* sp. (CCY 0311) cells that are adhering to each other clearly show

differences in internal cell organelle structure. (C) Two large lipid bodies (red arrows) can be identified in this *Phaeodactylum tricornutum* (CCY0033) cell. Red stippled lines indicate where OPL profiles were measured across the lipid bodies, the yellow where an OPL profile for, most likely, a chloroplast was measured. (D) An acid-cleaned diatom frustule of *Pinnularia borealis* (University of Gent, Belgium), and (E) a frustule of *Pinnularia* sp. (University of Antwerp, Belgium) cleaned with HNO_3. (F) A sample of the same *Pinnularia* sp. as in (E), that has been cleaned and dried with an alternative procedure (using H_2O_2).

Fig. 4. (A) Quantitative phase image and (B) its false-colour 3D rendition obtained with an oLine D^3HM of the chain-forming diatom *Melosira* sp.. The profiles in (A) correspond to profiles shown in (C) of optical path length. Profiles have been taken through cells fully and partially packed with chloroplasts as well as through mucus pads that are occasionally found to connect cells.

Fig. 5. Combination of DHM and fluorescence. The chain-forming diatom *Melosira* sp. (CCY0408) is imaged with the QMod set-up on an epifluorescent microscope (fluorescence emission at ≥520 nm): (A) Hologram, (B) light intensity image, (C) phase image with arrows indicating the presence of mucus pads connecting cells, and (D) algal autofluorescence. (E) and (F) are the merged images of the light and phase images, respectively, with the autofluorescence showing the lack of fluorescence from some of the cells (numbered 1-4 in E).

Fig. 6. DHM phase information and viability. Representative examples of individual cells from two diatom cultures were imaged in their natural healthy state: (A) *Navicula* sp. (CCY 0311) and

(D) *Nitzschia cf. pellucida* (DCG 0303). Subsequent heat-killing shows changes in the OPL landscape of the cells for (B) *Navicula* and (E) *N. pellucida*. The white scalebar applies to all four images. (C) and (F) show OPL profiles drawn across the longest axes of the cells as exemplified with the white stippled lines.

Fig. 7. Box-whisker plots for the extracted features for live versus dead (heat-killed) cells of *Nitzschia cf. pellucida* (DCG0330): (A) morphology-based features, (B) textural features based on the light intensity (LI) information and (C) textural features based on the phase information (PI). Box-whiskers represent the following: means are shown, with the lower and upper box limits showing the 25th and 75th percentile, respectively. Whiskers show the range, whilst crosses represent outliers. The absence of a star (*) signifies statistical non-significance, whilst *** denotes a significant difference at the $p < 0.001$ level, ** a difference at the $p < 0.01$ level and * a difference at the $p < 0.05$ level.

Fig. 8. A biofilm has been formed by *Nitzschia capitellata* cells. The structure is more easily visualized with the false-colour phase images shown in (D) compared to the light intensity image (A). The arrow shows the edge of the biofilm sample. B–C: Diatoms moving within this biofilm create distinct trails where the differences in optical path length (OPL) of the trails are quantifiable in the false-colour phase images (E–F) compared to the light intensity image (B–C). C: Two cells and two trails were profiled (red lines) for OPL measurements discussed in the main text.

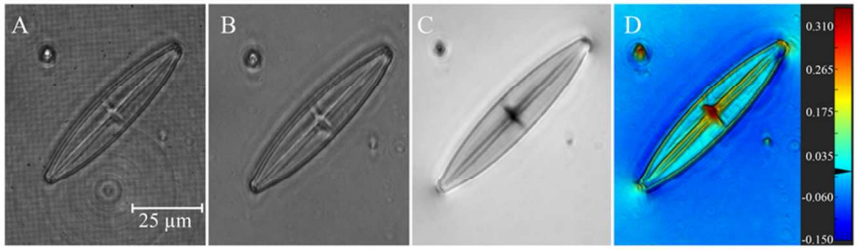

Fig. 1 (A) Hologram of a cleaned diatom frustule of *Stauroneis* sp. (University of Gent, Belgium) as obtained with a digital holographic microscope (oLine D^3HM). This hologram contains both light intensity information (B) as well as phase information (C) representing the optical path length (OPL) of the object. (D) The OPL of an object is more clearly visualized with false colouring of the phase information.
80x36mm (300 x 300 DPI)

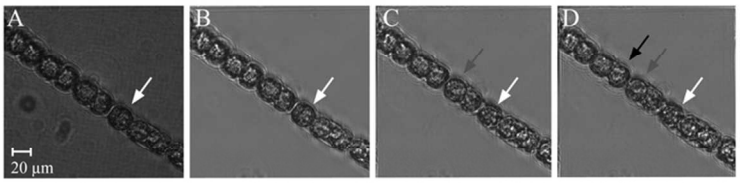

Fig. 2. Post-acquisition refocusing with the D^3HM of the cells in a *Melosira* sp. chain: (A) A single hologram is recorded of the whole chain of cells with the cell marked by the white arrow in focus. (B) The corresponding intensity image is derived from the hologram in the optimal focus plane for the cell marked by the white arrow. (C) Via hologram reconstruction, the focus plane is shifted by -10 µm to bring a cell to the left into focus (grey arrow). The corresponding intensity image is again derived. (D) A shift by -15 µm from the original focus plane brings the cell marked with the black arrow into focus, and the corresponding intensity image is shown. Note how the original cell (white arrow) gradually loses its focus as the focus plane shifts further away.
80x36mm (300 x 300 DPI)

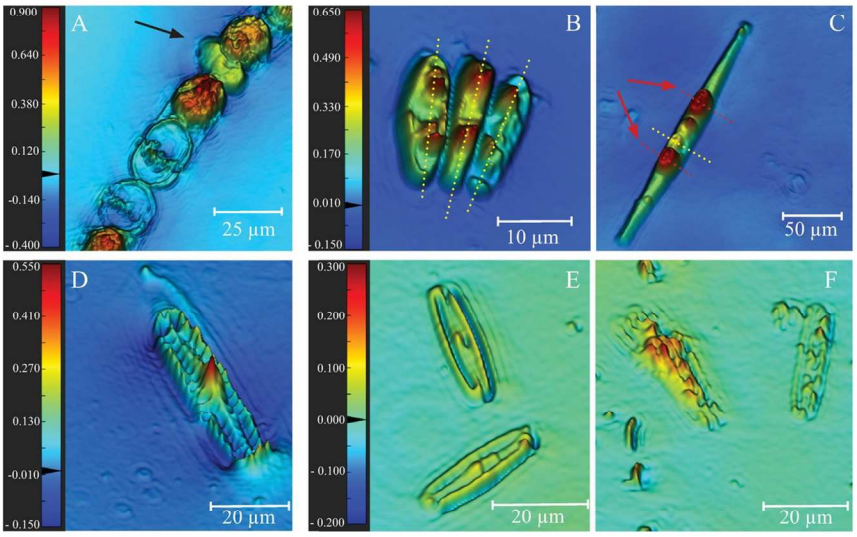

Fig. 3. Examples of false-coloured 3D renditions of the quantitative phase information captured with both the D^3HM (A,D–F) and the QMod (B–C) for a number of different diatoms. (A) The chloroplasts of the chain-forming diatom *Melosira* sp. (CCY0407, The Netherlands) often fill the cells to varying degrees, with empty cells being present along the chain. Cells are frequently connected by mucus pads, which are clearly distinguishable in this false-colour image (black arrow). (B) Three *Navicula* sp. (CCY 0311) cells that are adhering to each other clearly show differences in internal cell organelle structure. (C) Two large lipid bodies (red arrows) can be identified in this *Phaeodactylum tricornutum* (CCY0033) cell. Red stippled lines indicate where OPL profiles were measured across the lipid bodies, the yellow where an OPL profile for, most likely, a chloroplast was measured. (D) An acid-cleaned diatom frustule of *Pinnularia borealis* (University of Gent, Belgium), and (E) a frustule of *Pinnularia* sp. (University of Antwerp, Belgium) cleaned with HNO_3. (F) A sample of the same *Pinnularia* sp. as in (E), that has been cleaned and dried with an alternative procedure (using H_2O_2).
119x83mm (300 x 300 DPI)

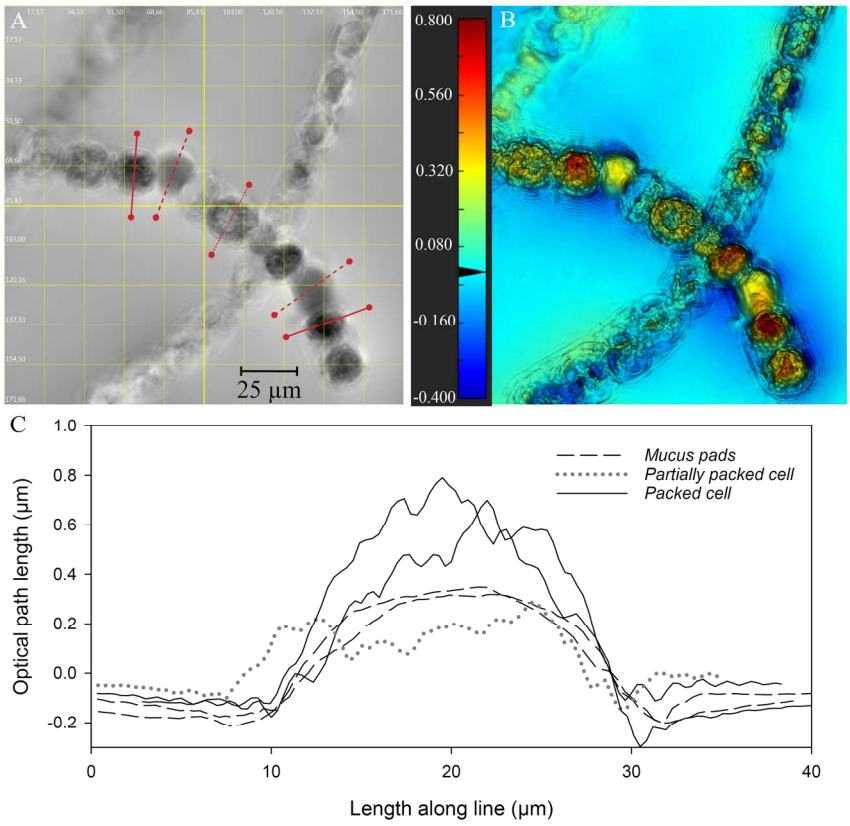

Fig. 4 (A) Quantitative phase image and (B) its false-colour 3D rendition obtained with an oLine D^3HM of the chain-forming diatom *Melosira* sp.. The profiles in (A) correspond to profiles shown in (C) of optical path length. Profiles have been taken through cells fully and partially packed with chloroplasts as well as through mucus pads that are occasionally found to connect cells.
170x170mm (300 x 300 DPI)

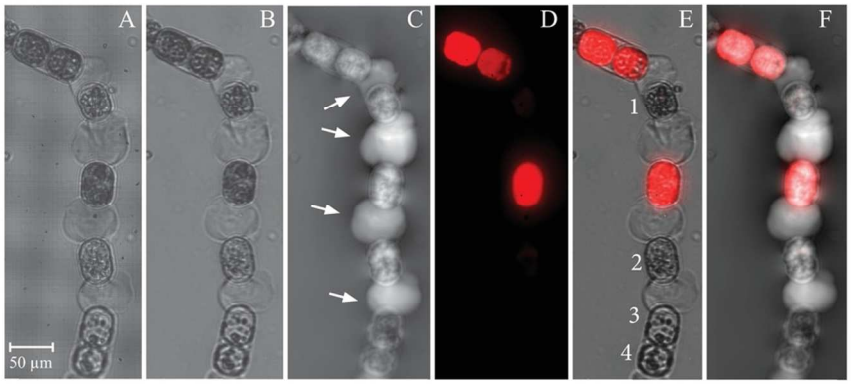

Fig. 5. Combination of DHM and fluorescence. The chain-forming diatom *Melosira* sp. (CCY0408) is imaged with the QMod set-up on an epifluorescent microscope (fluorescence emission at ≥520 nm): (A) Hologram, (B) light intensity image, (C) phase image with arrows indicating the presence of mucus pads connecting cells, and (D) algal autofluorescence. (E) and (F) are the merged images of the light and phase images, respectively, with the autofluorescence showing the lack of fluorescence from some of the cells (numbered 1-4 in E).
99x58mm (300 x 300 DPI)

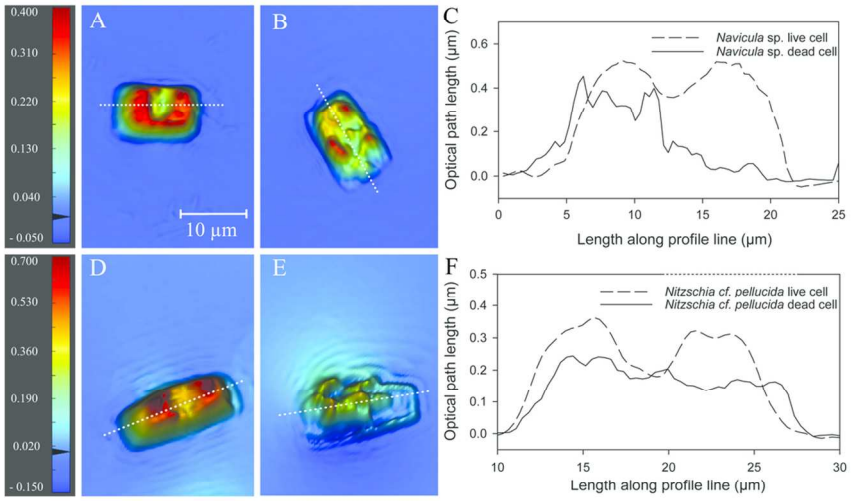

Fig. 6. DHM phase information and viability. Representative examples of individual cells from two diatom cultures were imaged in their natural healthy state: (A) *Navicula* sp. (CCY 0311) and (D) *Nitzschia cf. pellucida* (DCG 0303). Subsequent heat-killing shows changes in the OPL landscape of the cells for (B) *Navicula* and (E) *N. pellucida*. The white scalebar applies to all four images. (C) and (F) show OPL profiles drawn across the longest axes of the cells as exemplified with the white stippled lines.
109x71mm (300 x 300 DPI)

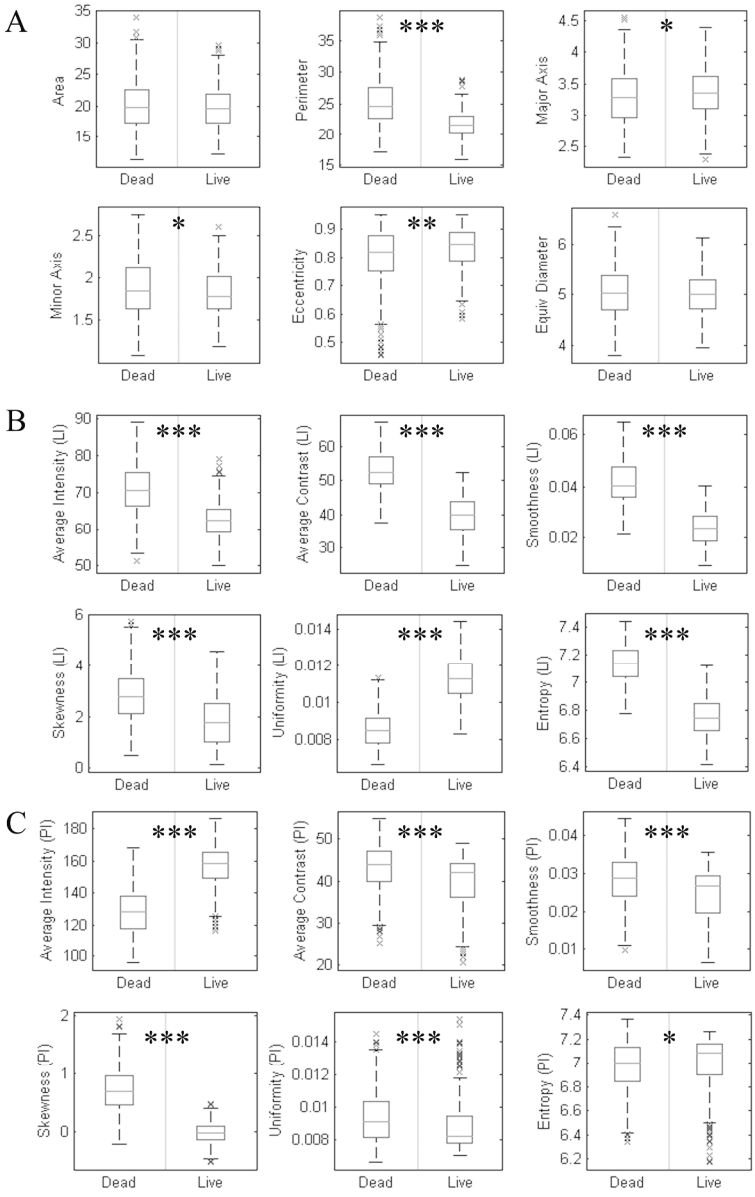

Fig. 7. Box-whisker plots for the extracted features for live versus dead (heat-killed) cells of *Nitzschia cf. pellucida* (DCG0330): (A) morphology-based features, (B) textural features based on the light intensity (LI) information and (C) textural features based on the phase information (PI). Box-whiskers represent the following: means are shown, with the lower and upper box limits showing the 25th and 75th percentile, respectively. Whiskers show the range, whilst crosses represent outliers. The absence of a star (*) signifies statistical non-significance, whilst *** denotes a significant difference at the $p < 0.001$ level, ** a difference at the $p < 0.01$ level and * a difference at the $p < 0.05$ level.
239x368mm (300 x 300 DPI)

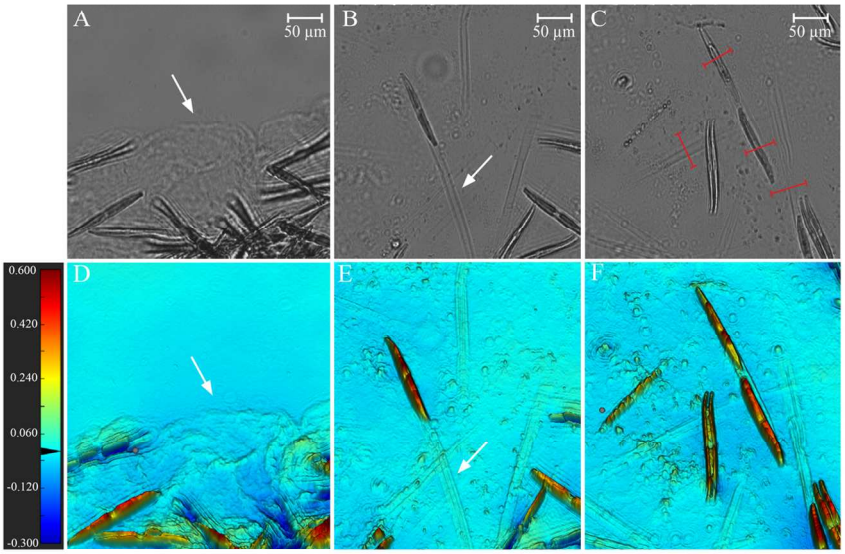

Fig. 8. A biofilm has been formed by *Nitzschia capitellata* cells. The structure is more easily visualized with the false-colour phase images shown in (D) compared to the light intensity image (A). The arrow shows the edge of the biofilm sample. B–C: Diatoms moving within this biofilm create distinct trails where the differences in optical path length (OPL) of the trails are quantifiable in the false-colour phase images (E–F) compared to the light intensity image (B–C). C: Two cells and two trails were profiled (red lines) for OPL measurements discussed in the main text.
129x97mm (300 x 300 DPI)